Salt Contribution to RNA Tertiary Structure Folding Stability

Zhi-Jie Tan[†‡] and Shi-Jie Chen[§¶*]

[†]Department of Physics and [‡]Key Laboratory of Artificial Micro- and Nano-Structures of the Ministry of Education, School of Physics and Technology, Wuhan University, Wuhan, People's Republic of China; and [§]Department of Physics and Astronomy and [¶]Department of Biochemistry, University of Missouri, Columbia, Missouri

ABSTRACT Accurate quantification of the ionic contribution to RNA folding stability could greatly enhance our ability to understand and predict RNA functions. Recently, motivated by the potential importance of ion correlation and fluctuation in RNA folding, we developed the tightly bound ion (TBI) model. Extensive experimental tests showed that the TBI model can lead to better treatment of multivalent ions than the Poisson-Boltzmann equation. In this study, we use the model to quantify the contribution of salt (Na^+ and Mg^{2+}) to the RNA tertiary structure folding free energy. Folding of the RNA tertiary structure often involves intermediates. We focus on the folding transition from an intermediate state to the native state, and compute the electrostatic folding free energy of the RNA. Based on systematic calculations for a variety of RNA molecules, we derive a set of formulas for the electrostatic free energy for tertiary structural folding as a function of the sequence length and compactness of the RNA and the Na^+ and Mg^{2+} concentrations. Extensive comparisons with experimental data suggest that our model and the extracted empirical formulas are quite reliable.

INTRODUCTION

To understand the functions of nucleic acids, we need to be able to quantitatively predict and analyze their folding. Nucleic acids are highly negatively charged molecules, and their folding into compact native structures involves a significant juxtaposition of negative charges on the backbone and a consequent significant charge-charge repulsion against folding. Metal ions are critical for tertiary structural formation of RNAs because the ions can neutralize backbone charge repulsion (1–15). In this work, we aimed to develop a theory to quantitatively predict the ion-dependent electrostatic contributions to the stability of RNA tertiary structural folding.

Most nucleic acids fold in a hierarchical and sequential manner (2,4). The secondary segments are formed first with strong Watson-Crick basepairing/stacking interactions, followed by the formation of tertiary structures in which helices and loops are juxtaposed to form a compact three-dimensional (3D) structure (1,2,4). An RNA sequence may form multiple secondary structures and consequently multiple tertiary structures. Furthermore, with the help of metal ions, RNA tertiary structure folding could also involve rearrangement of the secondary structures (16,17). Therefore, RNA folding can involve a complex dependence on metal ions. To understand how ions facilitate the formation of RNA tertiary structures, we need to quantify the different energetic components of this process, including the conformational entropy, the basepairing/stacking interaction energy, the ion-mediated global electrostatic energy, and the free energy for specific tertiary contacts. These different components are coupled. However, as an approximation, for the purpose of investigating the ion dependence of folding stability, we focus here on the electrostatic effects.

For the formation of secondary structural segments, the thermodynamic parameters at a standard salt condition (i.e., 1 M Na^+) have been experimentally determined. These parameters form the basis for the predictions of RNA and DNA secondary structures and folding kinetics (18–21). Moreover, for other, nonstandard ionic conditions, experimental and theoretical studies have produced a series of energetic parameters for helices (19,22–27) and loops (25). However, for tertiary structure folding, our ability to quantitatively predict the ion effect on folding stability is still very limited (1–15). Our goal in this work was to develop a theory to quantify the ion dependence of tertiary structural folding stability.

Because RNA tertiary structure folding involves a very high charge density on backbone and very complex structures, the ion effect can be particularly complex (28–38). For a long time, there have been two polyelectrolyte theories: the counterion condensation (CC) theory (28) and the Poisson-Boltzmann (PB) theory (29–33). For complex RNA tertiary structures, the straight line-charge model used in the CC theory is not applicable (28). Furthermore, the RNA charge buildup in tertiary structures can cause a significant accumulation of cations around the RNA. Theoretical and experimental studies suggest that the accumulation of multivalent ions such as Mg^{2+} around nucleic acids could potentially cause a strong correlation (coupling) of ions (8,34,35,62) in the vicinity of RNAs, i.e., the potential acting on an ion is a function not only of the coordinates that define the position of the ion but also of the instantaneous configuration of the other ions. For example, in an experiment involving Mg^{2+}-induced compaction in a tethered DNA duplex system (62), it was found that the

Submitted April 22, 2011, and accepted for publication May 23, 2011.

*Correspondence: chenshi@missouri.edu

Editor: Samuel Butcher.

0006-3495/11/07/0176/12 $2.00

doi: 10.1016/j.bpj.2011.05.050

PB-predicted midpoint [Mg^{2+}] value required for duplex compaction was 10 times higher than the experimentally measured value, and inclusion of the correlation effect led to significantly improved predictions (8). The PB theory ignores such ion-ion correlations, which could provide an important electrostatic force in stabilizing a tertiary fold.

To take into account the effects of ion correlations and the ion-binding ensemble, we developed the tightly bound ion (TBI) model (39). Extensive experimental comparisons showed that the inclusion of ion correlation and fluctuation leads to improved predictions for the thermodynamic stability of DNA and RNA helices (25–27), and DNA helix-helix assembly (40–43). Recently, this model was refined to treat complex DNA/RNA structures with atomic detail, and was shown to give reliable predictions of ion-binding properties for a variety of DNA and RNA structures (44).

In this work, we used the TBI model to calculate the effects of Na^+ and Mg^{2+} on the stabilization of RNA tertiary structures. Through systematic calculations for a variety of RNA structures, we derived a set of empirical formulas to quantify the contributions of Na^+ and Mg^{2+} to the stability of RNA tertiary structure folding. Our predictions and empirical formulas are compared with and supported by extensive experimental measurements.

METHODS

General description

Under different ionic conditions, an RNA can have different stable states. We consider three states: unfolded, intermediate, and native (folded). At a low ion concentration, the RNA forms an unfolded state due to the strong Coulombic repulsion of the backbone. The unfolded state is an ensemble of fluctuating coil-like conformations. At a moderate ion concentration, the RNA is partially neutralized and the Coulombic repulsion is reduced. As a result, the secondary structure (helices and loops) can be formed and stabilized by basepairing/stacking interactions. We call such a structure the intermediate state $\mathcal{I}$. At a low/moderate ion concentration, the formation of the helices is accompanied by a larger accumulation of backbone charges (compared with a single-stranded chain), and charge neutralization may not be strong enough to cause the formation of stable tertiary interactions. When the ion concentration becomes sufficiently high, an ion-mediated interaction leads to a higher frequency of close proximity between secondary structural subunits (helices and loops). Thus, ions promote the transition from the intermediate state to the compact native state $\mathcal{N}$. Based on the folding model described above, as an approximation, we model the tertiary folding process as the transition from the intermediate ($\mathcal{I}$) state to the native ($\mathcal{N}$) state (45,46):

$$\mathcal{I} \rightarrow \mathcal{N}. \tag{1}$$

The electrostatic free energy $\Delta G^E(Na^+, Mg^{2+})$ for the tertiary structure folding can be characterized by the free-energy difference between the native and intermediate states (45,46):

$$\Delta G^E_{Na^+,Mg^{2+}} = G^E_{Na^+,Mg^{2+}}(\mathcal{N}) - G^E_{Na^+,Mg^{2+}}(\mathcal{I}), \tag{2}$$

where $G^E_{Na^+,Mg^{2+}}(\mathcal{N})$ and $G^E_{Na^+,Mg^{2+}}(\mathcal{I})$ are the electrostatic free energies for the native and intermediate states, respectively. To quantify the Mg^{2+} effect, we separate out the contribution $\Delta\Delta G_{Mg^{2+}}$ of Mg^{2+} ions in tertiary structure folding from $\Delta G^E_{Na^+,Mg^{2+}}$ (45,46):

$$\Delta\Delta G_{Mg^{2+}} = \Delta G^E_{Na^+,Mg^{2+}} - \Delta G^E_{Na^+,Mg^{2+}=0}, \tag{3}$$

where $\Delta G^E_{Na^+,Mg^{2+}}$ and $\Delta G^E_{Na^+,Mg^{2+}=0}$ are the electrostatic tertiary structure folding free energies in the presence and absence of Mg^{2+}, respectively. We use the recently developed atomistic TBI model to evaluate the electrostatic free energy $\Delta G^E_{Na^+,Mg^{2+}}$ (44).

Structural models

To evaluate the ion electrostatic effects, we first need to build the 3D atomic structures for the different states.

Native structures

We obtained the following native structures for the RNAs studied in this work from the Protein Data Bank (PDB): beet western yellow virus (BWYV) pseudoknot (PDB code: 437D) (48); a 58-nt fragment of large subunit ribosomal RNA (rRNA) from *E. coli* (nucleotide 1051–1108, PDB code: 1HC8) (49); yeast $tRNA^{Phe}$ (PDB code: 1TRA) (50); T2 gene 32 mRNA (T2) pseudoknot (PDB code: 2TPK) (51); and mouse mammary tumor virus (MMTV) frameshifting pseudoknot (PDB code: 1RNK) (52). For the HIV-1 kissing complexes studied here (53), because of the similarity in the sequences and basepairing/coaxial-stacking patterns, we used the structure of HIV-1(MAL) genomic RNA DIS (54) (PDB code: 2B8S) to model the 3D structures of the HIV-1_{Lai} DIS kissing complexes (45,53,54). We also studied the T4 gene mRNA pseudoknot and its variant (T4-35 and T4-32 pseudoknots) with 35 and 32 nucleotides, respectively. Table 1 summarizes the above RNAs, and Fig. 1 shows their 3D structural models.

Intermediate structure

Strictly speaking, the intermediate state is an ensemble of conformations with secondary structural segments (helices and loops) with flexible configurations/orientations. For example, pseudoknot folding often involves hairpin as an intermediate state with dangling, single-stranded tails, whereas the folding intermediate of a kissing complex can be the unkissed hairpins with their respective fluctuating loop conformations. However, modeling of the whole conformational ensemble for such an intermediate state at the atomic level is computationally demanding. In this work, following the approach used in previous studies (22,45,46), we model the mean electrostatic properties for an intermediate state using an effective N_0-nt RNA helix. The total electrostatic free energy for an intermediate state of a N-nt RNA is approximated by $G^E(\mathcal{I}) = N \times g^E = N \times G^E(\text{Helix})/N_0$ (45,46). Here, given the short helices in the intermediate states (1,48–54), we choose N_0 = 24-nt (i.e., 12 bp). We produced the atomic structures of the A-form RNA helix for modeling the intermediate state using X3DNA software (55). The control tests on the effect of the approximate structural model for the intermediate states suggest that the predictions are not very sensitive to the selection of N_0 around 24-nt (see "Effect of the structural model for intermediate states" below). We note that a similar approximation was used and gave good results in previous studies on the effects of salt on hairpin stability (22), RNA tertiary structure folding (45,46), and the stability of HIV DIS Lai type kissing complex (44,47).

TBI model

The high concentration of counterions near the RNA surface could potentially cause strong correlation (coupling) between the ions. Such an effect is stronger for multivalent ions. To account for this potentially important effect, we classify the multivalent ions into two types (39–44): tightly bound (TB; strongly correlated) and diffusively bound (weakly correlated). The corresponding spatial regions are called the TB region and the diffusive region, respectively. It is important to note that the TB ions are mobile and involve no site-specific binding. For the TB ions, we enumerate discrete ion distributions to account for the correlation effect. For the diffusively bound

TABLE 1 The RNA molecules used in the study

RNAs	N (nt)	Experiment ref.	PDB ID and ref.	r_g*	Ref. salt†	$-\Delta H^\circ$ (kcal/mol)‡	$-\Delta S^\circ$ (cal/mol.K) ‡	$-\Delta G^\circ_{37}$ (kcal/mol)‡
BWYV pseudoknot	29	(12)	437D (48)	1.19	0.2 M Na^+	55	160.3	5.3
58-nt rRNA	58	(56)	1HC8 (49)	1.49	-	-	-	-
Yeast $tRNA^{Phe}$	76	(57)	1TRA (50)	1.37	-	-	-	-
HIV-1_{type} kiss complex§	42	(53)	2B8S (54)	1.05	1 M Na^+	68.0	175.8	13.5
T2 pseudoknot	36	(58)	2TPK (51)	1.11	0.1 M K^+	47.0	147.3	1.3
MMTV pseudoknot	33	(59)	1RNK (52)	0.97	1 M Na^+	40.6	117.3	4.2
T4-35 pseudoknot	35	(60)	-	1.05¶	60 mM Na^+	70.0	210.4	4.7
T4-32 pseudoknot	32	(60)	-	1.10¶	60 mM Na^+	58.0	176.0	3.4

*$r_g = R_g/R^0{}_g$, where R_g and $R^0{}_g$ represent the radii of gyration of a RNA tertiary structure and the corresponding A-form RNA duplex with the same chain length, respectively. Larger $R^0{}_g/R_g$ corresponds to more-compact tertiary structure folding (44).

†Thermodynamic data for the reference salt conditions are experimentally available.

‡Thermodynamic data are taken from the experiments at the reference salt conditions.

§As an approximation, we use the wide-type HIV-1_{Lai} (54) to model the HIV-1_{type} kissing complex (53) because they have similar kissing interfaces, stems, and unkissing hairpins (44).

¶3D atomic structures are not available in the PDB and NDB. We assume $R^0_g/R_g \simeq 1.04$ and 1.1 for T4-35 and T4-32, respectively, because T4-35 has longer tails than the T2 pseudoknot, whereas T4-32 is similar to the T2 pseudoknot in structural compactness (58,60).

ions, we use the mean-field (PB) equation. We treat the monovalent ions, whose correlation effect is negligible, as a diffusive ionic background.

To enumerate the ion distributions for the TB ions, we discretize the TB region into cells, each around a phosphate, and describe the ion distribution (also called the ion-binding mode) in a coarse-grained representation (as the number of ions in each cell). The total partition function Z for the TB ions is given by the summation over all the possible binding modes M: $Z = \sum_M Z_M$, where Z_M is the partition function for a binding mode M. The electrostatic free energy for a given RNA structure is determined as $G^E = -k_BT \ln \sum_M (Z_M)$. Details about the numerical computation and the parameter sets are described in the Supporting Material. As illustrated in Fig. S6, because the correlation effect causes the TB ions to self-organize and form the low-energy states

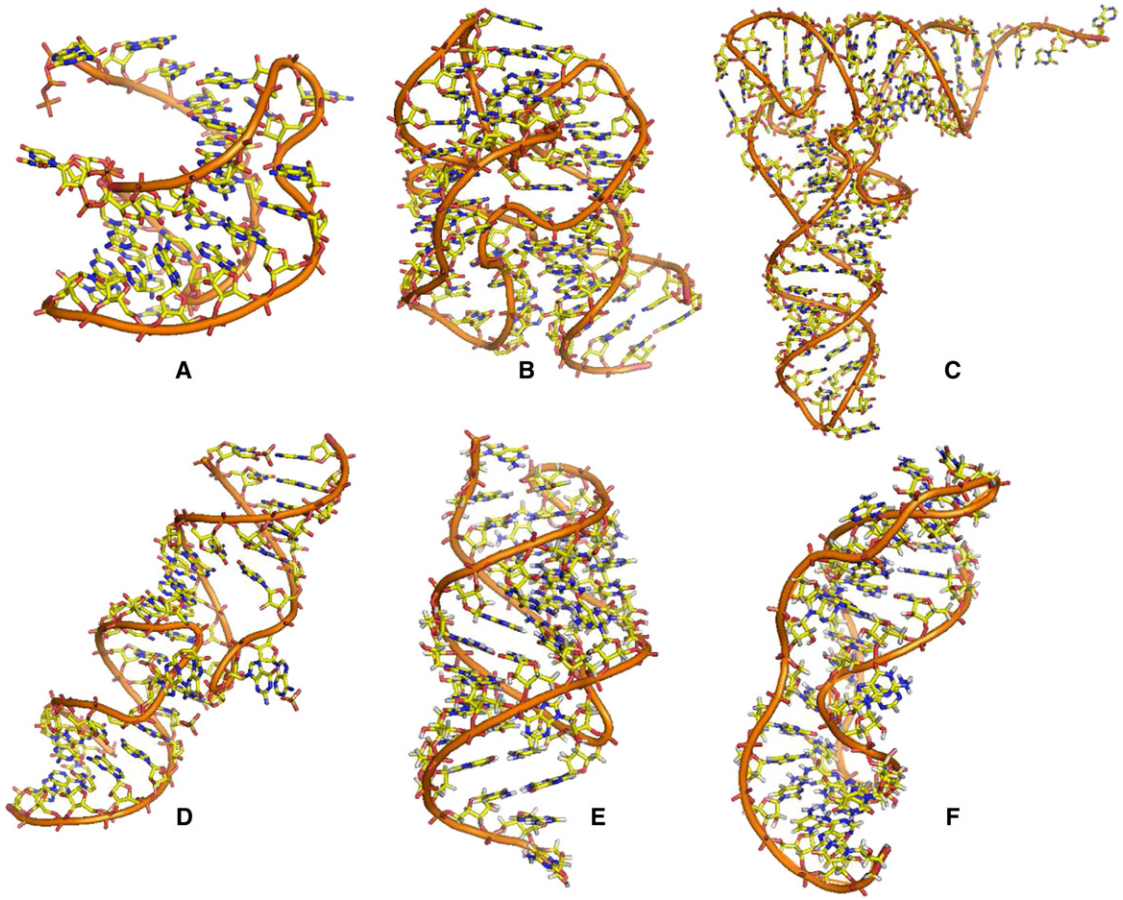

FIGURE 1 (*A–F*) Illustrations of 3D atomic RNA structures: (*A*) BWYV pseudoknot (PDB code: 437D) (48); (*B*) a 58-nt rRNA fragment (PDB code: 1HC8) (66); (*C*) yeast tRNAPhe (PDB code: 1TRA) (50); (*D*) HIV-1 Lai DIS kissing complex (PDB code: 2B8S) (54); (*E*) T2 gene 32 mRNA (T2) pseudoknot (PDB code: 2TPK) (51); and (*F*) MMTV frameshifting pseudoknot (PDB code: 1RNK) (52). See also Table 1.

that cannot be reached by the mean-field states, the TBI model may give improved predictions for RNA-Mg^{2+} interactions (44).

RESULTS AND DISCUSSION

We investigate the ion-dependent folding free energy for a series of RNAs of chain length from 29 nt to 76 nt in a solution with [Na^+] varying from 1 mM to 3 M, and [Mg^{2+}] from 0.1 μM to 0.1 M. We derive empirical formulas for the electrostatic folding free energies as functions of RNA chain length, structural compactness, and [Na^+] and [Mg^{2+}]. The empirical formulas are then compared with and validated by extensive experimental data for a variety of RNA structures (12,53,56–60).

To quantitatively describe the compactness of the RNA structure, we introduce a parameter $r_g = (R_g{}^0/R_g)$, where R_g and $R_g{}^0$ are the radii of gyration of the folded (native) RNA structure and the corresponding A-form RNA duplex with the same chain length (44), respectively. The $r_g(= R_g{}^0/R_g)$ parameters for the RNAs used in the study are shown in Table 1.

Electrostatic contribution to RNA tertiary structure folding

The electrostatic free energies for tertiary structural folding are shown in Figs. 2 and 3 for three RNAs (BWYV pseudoknot, 58-nt rRNA fragment, and yeast $tRNA^{Phe}$), and in Fig. S7 and Fig. S8 for three other RNAs (T2 gene 32 mRNA pseudoknot, MMTV pseudoknot, and HIV-1 DIS-type kissing complex). In the following, we analyze the general and specific features of the different RNAs at different ionic conditions (pure Na^+, pure Mg^{2+}, and mixed Na^+/Mg^{2+} solutions, respectively). To compare the ion effects between the RNAs with different sequence lengths (Ns), we compute the electrostatic free energy per nucleotide: $\Delta g^E_{Na^+,Mg^{2+}} = \Delta G^E_{Na^+,Mg^{2+}}/N$ and $\Delta\Delta g_{Mg^{2+}} = \Delta\Delta G_{Mg^{2+}}/N$ (see Eqs. 2 and 3).

In a Na^+ solution

The different RNAs show similar [Na^+]-dependent behavior. As shown in Fig. 2 *A* and Fig. S7 *A*, the increase in [Na^+] results in a decrease in the electrostatic folding free energy Δg^E, and thus favors the RNA tertiary structure folding. When [Na^+] exceeds a certain high value (~0.5 M), the decrease of Δg^E versus [Na^+] slows down. This relation of Δg^E versus [Na^+] comes from the effect of Na^+ binding and neutralization. With the increase of [Na^+], the entropic cost for Na^+ binding is lowered and hence more Na^+ ions are distributed in the vicinity of RNAs, causing a stronger charge neutralization. The Na^+ neutralization is more pronounced for the compact native state than for the intermediate state, resulting in a decrease of Δg^E and a higher folding stability. When [Na^+] becomes high enough, the RNA backbone becomes nearly fully neutralized, and further addition of Na^+ does not cause significant changes. Therefore, the change of Δg^E with [Na^+] slows down at high [Na^+].

The different RNAs also exhibit different features of Δg^E versus [Na^+]. As shown in Fig. 2 *A*, the [Na^+] dependence of Δg^E for BWYV pseudoknot is much weaker than for 58-nt rRNA and yeast $tRNA^{Phe}$. For example, for BWYV pseudoknot, the decrease of [Na^+] from 1 M to 10 mM leads to the increase of Δg^E by ~0.13 kcal/mol, whereas for the 58-nt rRNA and yeast $tRNA^{Phe}$, the increases in Δg^E are ~0.39 kcal/mol and ~0.4 kcal/mol, respectively. The different behavior of the [Na^+] dependence can be attributed to the different structural compactness and chain lengths. BWYV pseudoknot is a small RNA (29 nt) with a slightly compact structure (r_g ~1.19), and thus the difference in charge density between the native and intermediate states is not significant. As a result, Δg^E of BWYV appears weakly dependent on [Na^+]. In contrast, the 58-nt rRNA has a very compact native structure (r_g ~1.49) (49), and the native state has a much higher backbone charge density than the intermediate state. Consequently, Δg^E of 58-nt rRNA exhibits a much stronger [Na^+] dependence. Compared with the 58-nt rRNA, $tRNA^{Phe}$ has a longer molecular length (76 nt) and slightly less compact native structure (r_g ~1.37). Fig. 2 *A* shows that the [Na^+] dependence of Δg^E for $tRNA^{Phe}$ is similar to that for the 58-nt rRNA fragment.

The specific [Na^+]-dependent behaviors discussed above suggest that the Na^+ contribution to RNA tertiary structure folding is dependent not only on [Na^+] but also on the structural compactness and chain length.

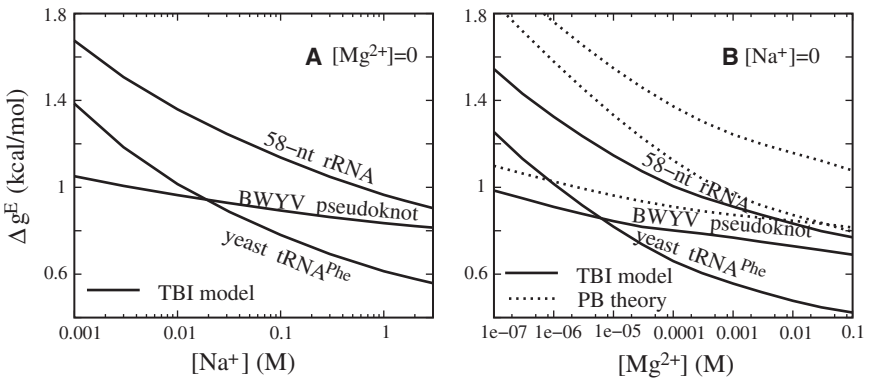

FIGURE 2 Electrostatic folding free energy $\Delta g^E = (\Delta G^E/N)$ for BWYV pseudoknot, 58-nt rRNA fragment, and yeast $tRNA^{Phe}$ for pure Na^+ (*A*) and Mg^{2+} (*B*) solutions at room temperature. Solid lines: TBI model; dotted lines: PB theory.

In a Mg^{2+} solution

As shown in Fig. 2 *B* and Fig. S7 *B*, the electrostatic folding free energy Δg^E for RNAs in Mg^{2+} solutions exhibits a Mg^{2+} dependence similar to that observed in the Na^+ solution. The increase in $[Mg^{2+}]$ leads to decreases in Δg^E, and thus favors folding into the compact tertiary structure. This can be attributed to the lowered Mg^{2+}-binding entropic penalty and hence stronger Mg^{2+} binding at higher $[Mg^{2+}]$. This leads to a lower Δg^E and higher folding stability.

Analogously to the folding in Na^+ solutions, the Δg^Es for the three RNAs also exhibit different behaviors for the $[Mg^{2+}]$ dependence. BWYV pseudoknot shows a much weaker $[Mg^{2+}]$ dependence of Δg^E than the 58-nt rRNA fragment and $tRNA^{Phe}$, whereas the 58-nt rRNA and $tRNA^{Phe}$ have a similar $[Mg^{2+}]$ dependence of Δg^E. This RNA-specific $[Mg^{2+}]$ dependence can be attributed to the RNA-specific structural compactness and chain length. An RNA with compact structures and long sequence can have a stronger ion dependence of the folding free energy.

Despite the qualitative similarity in Na^+- and Mg^{2+}-dependent folding free energies, the $[Mg^{2+}]$ dependence of Δg^E shows several distinctive features. First, Mg^{2+} is much more effective than Na^+ at achieving the same folding stability (Δg^E), and the high efficiency of Mg^{2+} is much more pronounced in tertiary structural folding than in secondary structural folding. For example, for $tRNA^{Phe}$, 0.3 mM Mg^{2+} can cause the same stability (Δg^E) as 1 M Na^+. In contrast, it requires 10 mM Mg^{2+} to cause the same folding stability for the secondary structure segments (25–27) as 1 M Na^+. Furthermore, we find that Mg^{2+} can cause low folding free energies that cannot be reached in a Na^+ solution even with high $[Na^+]$ ($\leq$3 M). For example, for $tRNA^{Phe}$, Δg^E at 10 mM Mg^{2+} is $\sim -0.2\ k_BT$ lower than at 1 M Na^+, and $\sim -0.1\ k_BT$ lower than at 3 M Na^+. This phenomenon suggests that Mg^{2+} tends to promote the formation of more-compact structures.

The above specific behavior for Mg^{2+} can be attributed to the high charge of Mg^{2+}, which causes stronger ion-phosphate and ion-ion interactions. The stronger ion-phosphate attraction leads to a stronger Mg^{2+} binding. On the other hand, the ion-ion correlations can drive Mg^{2+} ions to self-organize to reach the low-energy state below the mean-field state. Such effects are more pronounced for a more compact tertiary structure, which induces a higher $[Mg^{2+}]$ around RNA and hence stronger ion-ion correlations. Therefore, Mg^{2+} ions are much more efficient than Na^+ in stabilizing RNA tertiary structure folding, especially for compact structures.

In a mixed Na^+/Mg^{2+} solution

Fig. 3, *A–C*, show Δg^E as a function of $[Mg^{2+}]$ with the different $[Na^+]/Mg^{2+}$ mixture ratios for the BWYV pseudoknot, 58-nt rRNA fragment, and yeast $tRNA^{Phe}$, respectively. In similarity to the formation of RNA/DNA secondary structural segments (helix and loop) (26,44), the $[Mg^{2+}]$ dependence of the Δg^E exhibits three distinctive regimes owing to the competition between mono- and

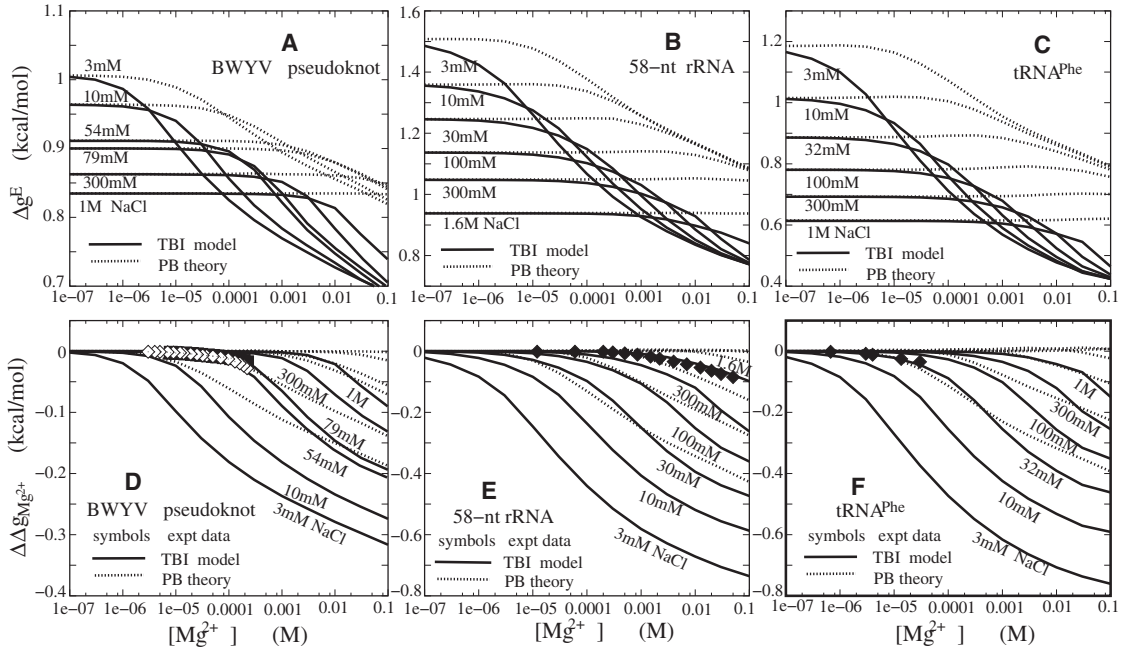

FIGURE 3 Electrostatic folding free energy $\Delta g_E = (\Delta G_E/N)$ (*A–C*) and Mg^{2+} contribution $\Delta\Delta g_{Mg^{2+}}$ to tertiary structure folding free energy (*D–F*) for BWYV pseudoknot (*A* and *D*), 58-nt rRNA fragment (*B* and *E*), and yeast $tRNA^{Phe}$ (*C* and *F*) for mixed Na^+/Mg^{2+} solutions at room temperature. Solid lines: TBI model; dotted lines: PB theory. Symbols (experimental data): (*D*) ◇ BWYV pseudoknot in 0.054 M Na^+; ◆ BWYV pseudoknot in 0.079 M Na^+ (66); (*E*) ◆ 58-nt rRNA fragment in 1.6 M monovalent ion solution (45,46,56); and (*F*) ◆ yeast $tRNA^{Phe}$ in 0.032 M Na^+ (45,57).

divalent ion binding (44,61): 1) When $[Mg^{2+}]$ is very low, Δg^E is nearly invariant and is equal to that in a pure Na^+ solution (see Figs. 2 *A* and 3, *A–C*, for comparison). 2) When $[Mg^{2+}]$ is further increased and exceeds a critical concentration (C_c), Δg^E decreases (with the increase of $[Mg^{2+}]$). C_c is higher for a higher mixed $[Na^+]$. 3) When $[Mg^{2+}]$ becomes very high, Δg^E exhibits a weak dependence on the mixed $[Na^+]$. This $[Na^+]/[Mg^{2+}]$ dependence comes from the interplay between Na^+ binding and Mg^{2+} binding (44). For very low $[Mg^{2+}]$, Mg^{2+} binding is suppressed by the strong Na^+ binding due to the low (high) entropic cost for Na^+ (Mg^{2+}) binding. Thus, Na^+ dominates the RNA stability and Δg^E is close to that in a pure Na^+ solution with the same $[Na^+]$. As $[Mg^{2+}]$ is increased, Mg^{2+} binding to RNA gradually becomes significant. The Mg^{2+} binding competes with Na^+ binding. Thus, Mg^{2+} plays important roles in the electrostatic effects of RNA stability and Δg^E decreases. At high $[Mg^{2+}]$, Mg^{2+} binding is strong due to the low entropic cost upon binding and the higher charge of Mg^{2+} compared with Na^+ ions, and thus the Na^+ binding is suppressed. As a result, the RNA stability is dominated by Mg^{2+}, and Δg^E becomes less sensitive to $[Na^+]$. As shown in Fig. 3, Mg^{2+} competes strongly with Na^+, even in a solution with molar Na^+ concentration, due to its higher charge and consequently much higher binding affinity.

Mg^{2+} contribution to RNA tertiary structure folding

To illustrate the role of Mg^{2+} in stabilizing specific RNA tertiary structures, we calculate the Mg^{2+} contribution $\Delta\Delta g_{Mg^{2+}} (=\Delta\Delta G_{Mg^{2+}}/N)$ to the folding free energy through Eq. 3. As shown in Fig. 3, *D–F*, Mg^{2+} is highly efficient at stabilizing RNA tertiary structures, especially for the more-compact structures such as the 58-nt rRNA fragment and $tRNA^{Phe}$. The Mg^{2+} contribution is dependent not only on $[Na^+]$ but also on the structure compactness and chain length of RNA. For the more compact structures and longer RNAs, and in lower $[Na^+]$, Mg^{2+} provides a greater contribution in stabilizing the native RNA structures. This can be attributed to the ion-RNA attractions and Na^+/Mg^{2+} competition in binding. Mg^{2+} has a high valency of +2 and can be more efficient than Na^+ in stabilizing the RNA structure, as discussed above.

Fig. 3, *D–F*, also show that the predicted $\Delta\Delta g_{Mg^{2+}}$ agrees well with available experimental data for the BWYV pseudoknot, 58-nt rRNA fragment, and yeast $tRNA^{Phe}$ with $[Na^+]$ from 0.32 mM to 1.6 M (12,56,57), while the PB theory overestimates $\Delta\Delta g_{Mg^{2+}}$ and consequently underestimates the role of Mg^{2+}. As discussed above and in previous studies (62), the PB theory ignores ion-ion correlation and ion-binding fluctuations by assuming mean-field fluid-like ionic distributions, and hence underestimates the Mg^{2+} binding (44,61) and overestimates $\Delta\Delta g_{Mg^{2+}}$. In contrast, the TBI theory can account for the above effects and allows the ions, especially polyvalent ions such as Mg^{2+} ions, to form correlated distributions with much lower energy than a mean-field ion distribution can reach, and gives improved predictions on Mg^{2+} binding (39,44) and Mg^{2+}-mediated folding free energy (39–42,44).

This theory does not treat the possible specific binding effects. The simplification may be valid for the BWYV pseudoknot and $tRNA^{Phe}$, as suggested by previous studies (12,45,46). However, for the 58-nt rRNA fragment, a previous PB-based computational study suggested that specific binding of Mg^{2+} may play a role (45,46). The good agreement between theory and experiment suggests that for the RNAs studied here, specific ion binding may not play a dominant role in the overall stabilization of the global fold.

The ion dependence of ΔG_E for the six RNAs shows the following general properties: 1) The tertiary folding free energy depends not only on ion concentration but also on the structural compactness of the sequence length of the RNAs. For example, the tertiary folding stability of $tRNA^{Phe}$ and the 58-nt rRNA fragment show a much stronger ion-concentration dependence than the pseudoknots, because the folding of $tRNA^{Phe}$ and the rRNA fragment involves the strong compaction of multiple secondary fragments, whereas pseudoknots only involve the weak compaction with the binding of dangling tails during tertiary folding. 2) Mg^{2+} is much more efficient than Na^+ in stabilizing RNA tertiary folding stability. Mg^{2+} of millimolar concentration could cause higher tertiary folding stability than Na^+ of molar concentration.

Parameterizations for the salt contributions to RNA tertiary structure folding

In the above calculations, we showed that our predictions for the Mg^{2+} contribution ($\Delta\Delta g_{Mg^{2+}}$) to RNA tertiary structure folding agree well with the available experimental data. In similarity to the empirical formulas for DNA and RNA helices in various $Na^+(K^+)/Mg^{2+}$ solutions, we fit empirical formulas for the electrostatic free energy for the different RNA structures in terms of the compactness of the RNA structure and the logarithms of the cation concentrations (19,24,26,27). Based on the systematic calculations for six RNAs (BWYV pseudoknot, MMTV pseudoknot, T2 pseudoknot, kissing complex, 58-nt rRNA fragment, and yeast $tRNA^{Phe}$), we fit an empirical formula for ΔG^E as a function of $[Na^+]$, $[Mg^{2+}]$, and sequence length N (nt) and the compactness ($r_g = R_g^0/R_g$) of the structure.

In a Na^+ solution

Based on the systematic calculations for the different RNAs, we fit the following empirical formula for the electrostatic free energy ΔG^E (in kcal/mol) for RNA tertiary structure folding in pure Na^+ solutions:

$$\Delta G^E\left[Na^+\right] = \Delta G^E_{1M\ Na^+} + a_1 N \ln\left[Na^+\right] + b_1 N \ln^2\left[Na^+\right], \tag{4}$$

where $\Delta G_{1M\ Na^+}$ (in kcal/mol) is the folding free energy at standard 1 M Na^+ salt, and the coefficients a_1 and b_1 are

given in the Supporting Material. As shown in Fig. S7, Eq. 4 gives a good fit to the calculated ΔG^E in pure Na^+ solutions for the six RNAs at the different temperatures.

In a Mg^{2+} solution

For the tertiary structure folding in a pure Mg^{2+} solution, we have the following empirical formula for the electrostatic folding free energy:

$$\Delta G^E\left[Mg^{2+}\right] = \Delta G^E_{1M\ Na^+} + a_2 N \ln\left[Mg^{2+}\right] + b_2 N \ln^2\left[Mg^{2+}\right] + c_2 N T^*, \quad (5)$$

where the coefficients a_2, b_2, and c_2 are given in the Supporting Material, and T^* is the effective temperature T/298.15 K. Fig. S7 shows that Eq. 5 fits the calculated ΔG^E well for the six studied RNAs in pure Mg^{2+} solutions.

In a mixed Na^+/Mg^{2+} solution

For mixed Na^+/Mg^{2+} solutions, we fit the following empirical formula for the electrostatic folding free energy $\Delta G[Na^+/Mg^{2+}]$:

$$\Delta G^E\left[Na^+/Mg^{2+}\right] = x\Delta G^E\left[Na^+\right] + (1\text{-}x)\Delta G^E\left[Mg^{2+}\right] + N\Delta g_{12}, \quad (6)$$

where the first two terms represent the fractional contributions from Na^+ and Mg^{2+}, respectively, and x and the cross-term Δg_{12} are given in the Supporting Material. As shown in Fig. S8, Eq. 6 gives a good fit with the TBI calculations on $\Delta G^E[Na^+/Mg^{2+}]$. In addition, for BWYV pseudoknot, 58-nt rRNA fragment, and yeast $tRNA^{Phe}$, as shown in Fig. S9, the empirical formulas (Eqs. 3–6) give good predictions regarding the Mg^{2+} contributions $\Delta\Delta G_{Mg^{2+}}$ to RNA tertiary folding free energy as compared with the experimental data (12,56,57).

Many previous studies on ion-nucleic acid interactions relied on the preferential interaction coefficient to describe the ion uptake/release in the nucleic acid folding process (3,12,22,63–68). The preferential interaction coefficient provides a direct account of ion accumulation/exclusion around a nucleic acid. The theoretical calculation for the preferential interaction coefficient involves integration of the excess ion concentrations in the solution space, and requires a full calculation of the ion distribution using the TBI/PB models. To provide a computationally efficient estimate of the ion-dependent free energy, here we use the (bulk) ion concentrations to parameterize the free energy. Unlike the preferential interaction coefficient, which is directly related to the nonideality of the ionic solution due to the presence of the RNA, the empirical formulas derived above show the solution nonideality (due to ion-RNA interaction) in a more implicit way through the nonlinear terms of the logarithms of the ion concentrations. However, to unveil the quantitative relationship between the solution nonideality and the nonlinear expansions in the above formulas, we need to perform systematic calculations, and with high-salt concentrations these calculations are complicated due to the further nonideality of the ionic solution (see Conclusions and Discussion).

Na^+/Mg^{2+}-dependent RNA tertiary structure folding stability

In addition to the good agreement between our predictions and experimental data regarding the Mg^{2+} contribution to RNA tertiary structure folding free energy ($\Delta\Delta G_{Mg^{2+}}$), we further use the empirical formulas to predict the ion-dependent tertiary structure folding stability and compare the predictions with experimental results for a set of RNAs: BWYV pseudoknot, T4-35 and T4-32 pseudoknots, HIV-1 DIS-type kissing complex, MMTV pseudoknot, and T2 pseudoknot (see Table 1).

As an approximation, the total tertiary structure folding free energy ΔG can be decoupled into an electrostatic contribution $\Delta G^E[Na^+/Mg^{2+}]$ and a nonelectrostatic contribution ΔG^{NE} (26,27):

$$\begin{aligned}\Delta G\left[Na^+/Mg^{2+}\right] &= \Delta G^E\left[Na^+/Mg^{2+}\right] + \Delta G^{NE} \\ &= \left(\Delta G^E\left[Na^+/Mg^{2+}\right] - \Delta G^E\left[\text{expt. } Na^+\right]\right) \\ &\quad + \Delta G\left[\text{expt. } Na^+\right],\end{aligned} \quad (7)$$

where ΔG[expt. Na^+] is the available free energy at an experimental ionic (Na^+) condition, and $\Delta G^E[Na^+/Mg^{2+}] - \Delta G^E$[expt. Na^+] can be estimated from the above empirical formulas (Eqs. 4–6). If the tertiary structure folding is a two-state transition, the melting temperature T_m can be estimated from $\Delta G_{T=T_m} = 0$ (19).

BWYV pseudoknot

For BWYV pseudoknot, with the above parameterized salt extensions, we predict ΔG as functions of $[Na^+]$ and $[Mg^{2+}]$. As shown in Fig. 4, *A* and *B*, our predictions agree well with the available experimental data (12) for both Na^+ and mixed Na^+/Mg^{2+} solutions. For pure Na^+ solutions, the increase of $[Na^+]$ decreases ΔG, and thus enhances the folding stability due to the decrease in ion-binding penalty and hence the enhanced ion neutralization. For the mixed Na^+/Mg^{2+} solution, the increase of $[Mg^{2+}]$ causes a transition from Na^+-dominating stability to Mg^{2+}-dominating stability, and enhances the RNA tertiary stability. As discussed above and in previous studies (25,26,44), this transition comes from the interplay between Na^+ binding and Mg^{2+} binding.

The good agreement between the experimental data and our calculations without considering specific ion binding suggests that nonspecific ion binding may play a dominant electrostatic role in stabilizing this pseudoknot. This result is in accordance with a previous experimental analysis (12). Note that our predicted ΔG is the free-energy change

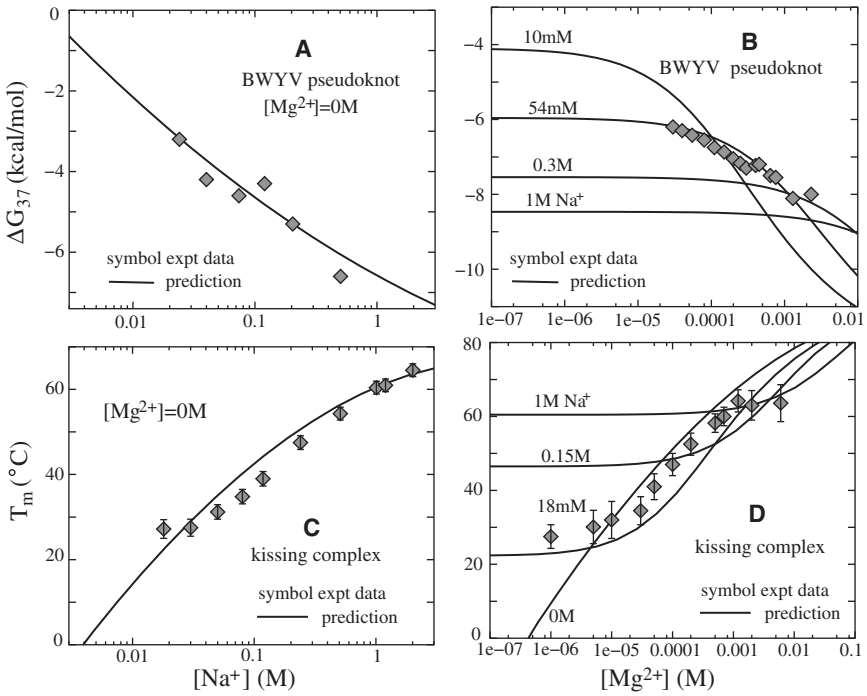

FIGURE 4 (*A* and *B*) Folding free energies ΔG_{37} at 37°C as functions of $[Na^+]$ (*A*) and $[Mg^{2+}]$ (*B*) for BWYV pseudoknot. Symbols (experimental data): (*A*) BWYV pseudoknot in pure Na^+ solutions (66), and (*B*) BWYV pseudoknot in a Mg^{2+} solution with 54 mM Na^+ ions (66). (*C* and *D*) T_m as a function of $[Na^+]$ (*C*) and $[Mg^{2+}]$ (*D*) for an HIV DIS-type kissing complex. Symbols (experimental data): (*C*) kissing complex in a pure Na^+ solution (44,53), and (*D*) kissing complex in Mg^{2+} solution with 18 mM Na^+ (44,53). The solid lines in panels *A–D* denote empirical formulas derived from the TBI model.

from the intermediate state (with secondary segments) to the native tertiary structure. The experiment suggests that there are two subtransitions from the secondary structure intermediate state to the native state for BWYV pseudoknot. Therefore, the total tertiary structure folding free energy is the sum of the two subtransitions (12).

Kissing complex

The kissing complex is a structurally and functionally important tertiary structural segment. The system may serve as a paradigm for loop-loop tertiary structural motif (1,2). Here, we estimate the Na^+- and Mg^{2+}-dependent stability for a 42-nt HIV DIS-type kissing complex (44,53).

Fig. 4, *C* and *D*, show the predicted T_m as functions of $[Na^+]$ and $[Mg^{2+}]$. The increases of $[Na^+]$ and $[Mg^{2+}]$ lead to increases of the melting temperature and the folding stability. The experimental comparisons show that our predictions can provide a quantitative estimation of the ion dependence of folding thermodynamics for the kissing complex in both Na^+ and Mg^{2+} solutions (53). At high $[Mg^{2+}]$, our predicted T_m is slightly higher than that in the experimental data (53). This may be a result of neglecting the conformational ensemble for the intermediate state, which would cause an underestimation of the conformational entropy of the separated hairpins and hence an overestimation of the kissing complex stability at high $[Mg^{2+}]$.

T4-35 and T4-32 pseudoknots

Based on the parameterized formulas, we estimate the folding stability for the T4-35 pseudoknot and its variant T4-32 pseudoknot. Fig. 5, *A* and *B*, show that our predicted free energies agree well with the available experimental measurements for the two RNAs (60). Specifically, adding Mg^{2+} ions leads to a decrease of the folding free energy ΔG and stabilization of the structure, and this enhancement is more pronounced for a larger molecule (e.g., T4-35).

Because the tertiary structure folding of the two pseudoknots is a standard two-state transition (60), we can readily estimate the melting temperature T_m. As shown in Fig. 5, *C* and *D*, our predicted T_ms are in good agreement with the experimental measurements (60), except for a slight overestimation at very high $[Mg^{2+}]$ ($\gtrsim$10 mM). The slight overestimation of the T_m at high $[Mg^{2+}]$ may be due to the simplification of the two-state model. Neglecting the conformational ensemble for the intermediate state may cause an underestimation of the conformational entropy, which could play an important role at high ion concentration and high temperature, causing a slight overestimation of T_m at high $[Mg^{2+}]$.

The 3D atomic structures for the two RNAs examined here are not available in the PDB or Nucleic Acid Database (NDB). In the calculations, we assume R_g^0/R_g ~1.05 and 1.1 for T4-35 and T4-32, respectively, because T4-35 has longer dangling ends than the T2 pseudoknot, and the structural compactness of T4-32 is similar to that of the T2 pseudoknot (58,60) (see Table 1). Our control tests indicate that the predicted results are not very sensitive to the slight change around the used values of R_g^0/R_g. In addition, as shown in Fig. 5, the ion dependence of the T4-35 pseudoknot is only slightly stronger than that of the T4-32 pseudoknot.

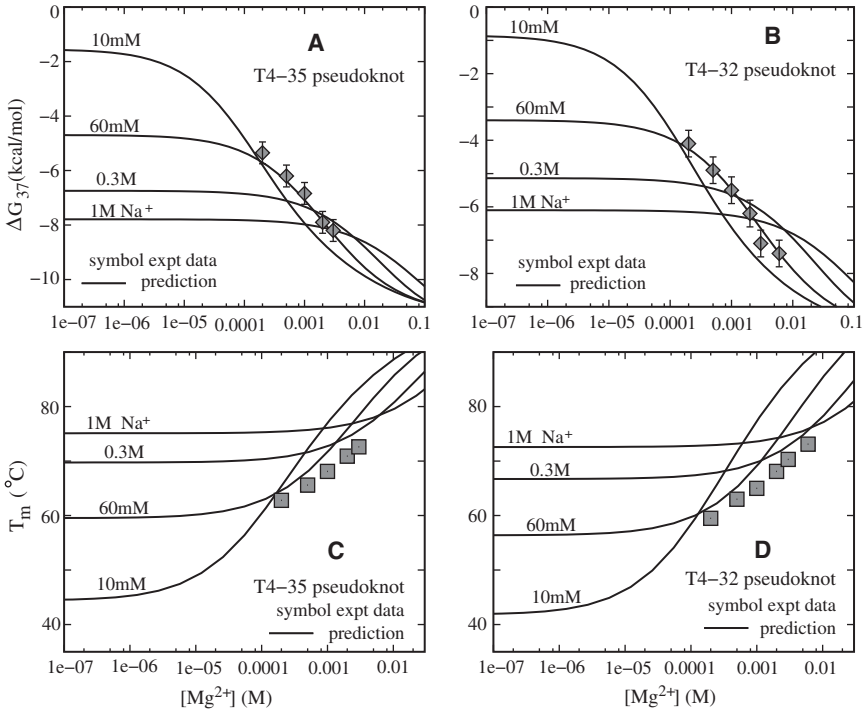

FIGURE 5 Folding free energies ΔG_{37} at 37°C (*A* and *B*) and T_m (*C* and *D*) as functions of $[Mg^{2+}]$ for T4-35 (*A* and *C*) and T4-32 (*B* and *D*) pseudoknots. Solid lines denote empirical formulas derived from the TBI model. Symbols (experimental data): (*A* and *C*) T4-35 pseudoknot in solution with 60 mM Na^+ ions (60). (*B* and *D*) T4-32 pseudoknot in Mg^{2+} solution with 60 mM Na^+ ions (60).

We also applied the above Na^+/Mg^{2+}-based empirical formulas to treat RNAs in K^+/Mg^{2+} solution and obtained good results (see Supporting Material and Fig. S10 for details). The slight deviations may come from the different specific binding affinities for Na^+ and K^+ (61,69–71).

Effect of the structural model for the intermediate states

Using a previously described approach (45,46), we model the average electrostatic properties of the intermediate state through an A-form helix with $N_0 = 24$ nt (see Materials and Methods). To examine the sensitivity of the predictions for the structural model of the intermediate state, we perform calculations using the different lengths of the A-form helix ($N_0 = 22$ nt, and 26 nt, respectively) for the intermediate state.

As shown in Fig. S11, we find that the predictions are not very sensitive to the selected A-form helix length N_0 (~24 nt) for the intermediate state. The increase of the A-form helix length N_0 only slightly weakens the ion-concentration dependence of the electrostatic free energy. For example, when N_0 is increased from 24 nt to 26 nt, for $tRNA^{Phe}$, Δg^E would decrease by 5% at 1 M Na^+ and by 6% at 0.01 mM Mg^{2+}. For Mg^{2+}, such a decrease in Δg^E would be $< 5\%$ at 10 mM Mg^{2+} and $< 7\%$ at 0.01 mM Mg^{2+}. Correspondingly, the Mg^{2+}-contribution $\Delta\Delta g_{Mg^{2+}}$ also decreases very slightly, and the maximum decrease occurs at high $[Mg^{2+}]$ when the Mg^{2+} accumulation around RNA is strongest. For $tRNA^{Phe}$ in a Mg^{2+} solution with mixed 32 mM Na^+, $\Delta g_{Mg^{2+}}$ increases by ~7% for 100 mM Mg^{2+} when N_0 is increased from 24 nt to 26 nt. For $[Mg^{2+}]$ lower than 100 mM, the decrease in $\Delta\Delta g_{Mg^{2+}}$ is even smaller. Furthermore, as shown in Fig. S11 *C*, the slight change in N_0 does not affect the good agreement between the predictions and the experimental data for $\Delta\Delta g_{Mg^{2+}}$ (12,45,56,57). From the above control tests, we find that the theoretical predictions are not very sensitive to the selected helix length, N_0 ~ 24 nt, for the intermediate state.

Nevertheless, the above model for the intermediate state is a simplified approximation. The realistic intermediate state should be represented as an ensemble of fluctuating conformations whose distribution is dependent on the ionic environment. Although the approximation gave useful results in this and previous studies, a rigorous, thorough study based explicitly on the complete conformational ensemble is needed to examine the validity of this simplified model. For example, would the approximation be more reliable for low or high ion concentrations? How is the ion condition coupled to the conformational ensemble heterogeneity and conformational entropy of the intermediate states? Neglecting the conformational ensemble for the intermediate state may cause the underestimation in the conformational entropy of RNA, which could play an important role at high ion concentration and high temperature, and may be responsible for the slight overestimation of T_m at very high $[Mg^{2+}]$. The current form of the model, however, cannot provide such a complete investigation because it would be computationally demanding to run the TBI computation for each and every conformation in the ensemble.

CONCLUSIONS AND DISCUSSION

In this work, we used the recently developed atomistic TBI model to quantify the contribution of ions (Na^+ and Mg^{2+}) to RNA tertiary structure folding stability. Based on systematic calculations on a series of RNAs, we derive empirical formulas to quantify the salt dependence of the RNA tertiary folding free energy. The predictions and empirical formulas derived from the theory agree with extensive experimental data. In addition, our study leads to the following conclusions:

1. The Na^+ and Mg^{2+} contributions to RNA tertiary structure folding free energy depend not only on the Na^+ and Mg^{2+} concentrations but also on the RNA chain length and structural compactness. Mg^{2+} plays a more important role in stabilizing more compact tertiary structure folding of longer RNA chains.
2. Mg^{2+} is much more efficient than Na^+ in stabilizing RNA tertiary structures (44,66). For example, for $tRNA^{Phe}$ and 58-nt rRNA fragment, 1 M NaCl and 0.3 mM $MgCl_2$ can make approximately the same contributions to the electrostatic free energy for tertiary structure folding, and Mg^{2+} of millimolar (~ mM) concentration can cause higher RNA tertiary stability than Na^+ of molar (~ M) concentration.
3. The TBI model gives better predictions regarding the Mg^{2+} contribution to RNA tertiary folding free energy than the PB theory, which underestimates the role of Mg^{2+} in stabilizing RNA tertiary structures, especially for the more compact tertiary structure folding with longer RNA chain.
4. Based on the results for a series of small RNAs, we can extract empirical formulas to quantify the Na^+ and Mg^{2+} contributions to RNA tertiary structure folding free energy. The formulas are validated by the extensive comparisons with experimental data, and thus may be reliable and practically useful.

The agreement between our predictions and the extensive experimental data suggests that the TBI model may provide a reliable treatment for predicting the electrostatic free energy of complex nucleic acid structures with atomic detail. However, in modeling RNA tertiary structure folding, we employ several important approximations.

First, the RNA tertiary structure folding is modeled as a two-state transition from the secondary structure as the intermediate state to the native state, and the mean electrostatic properties of intermediate state are modeled as those of a finite-length A-RNA helix. With such an approximation, we neglect the detailed structure and the conformational ensemble of the intermediate state, whose conformational distribution is dependent on the ion environment (66). Although the results of this work and previous studies suggest that the approximation may provide a useful lowest-order description for the structural ensemble-averaged properties in nucleic acid folding thermodynamics (22,44–46), a more accurate representation of the structures is required to determine how the structural details and conformational ensemble of the intermediate state affect the folding stability, as explained above and suggested by recent experiments (66).

Second, in the TBI model, we ignore specific binding and possible dehydration effects. Specific binding may play an important role in stabilizing specific tertiary structure through binding into specific pockets with specific chemical identity, although the effect may not be dominant for ion effects of the overall folding stability for the RNAs studied here. Furthermore, in the TBI model, we also ignore sequence-dependent ion binding. Ions can preferentially bind to C/G or A/T-rich sequences, and this effect is important for sequence-directed DNA/RNA bending (42,72). For the RNA molecules with generic sequence studied here, such an effect may not be significant.

Third, in the TBI model, we assume that the charges on an RNA are distributed only on phosphates, and other atoms are completely neutral. Such an approximation may be valid for the macroscopic electrostatic properties studied here, as suggested by the good theory-experiment agreement. However, further developments need to include more-detailed distributions of the specific (partial) charges of the RNA.

Finally, in modeling the salt solutions, we assume that ions are completely dissociated, and ignore the nonideality (such as ion pairing) of salt solutions (38). Such an approximation may be valid at low salt concentrations; however, for very high salt concentrations, due to cation-coion attractions, cations can form ion clusters with coions, and the effective valency of cations can be decreased (38). The nonideality of the solution would be effectively described by the activity instead of the concentration (67,68). Neglecting the nonideality could also cause an overestimation of the role of cations in stabilizing RNA tertiary structures at high salt concentrations, especially for multivalent solutions. Further development of the theory should include the effects of solution nonideality (38,67,68).

SUPPORTING MATERIAL

Additional text with equations, 12 figures, and references are available at http://www.biophysj.org/biophysj/supplemental/S0006-3495(11)00652-7.

This research was supported by the National Science Foundation (grants MCB0920067 and MCB0920411), National Institutes of Health (grant GM063732) (to S.-J.C.), National Science Foundation of China (grants 10844007 and 11074191), Program for New Century Excellent Talents (NCET 08-0408), Chutian Scholar Program of Hubei Province, and Fundamental Research Funds for the Central Universities and the Scientific Research Foundation for the Returned Overseas Chinese Scholars, State Education Ministry (to Z.-J.T.).

REFERENCES

1. Bloomfield, V. A., D. M. Crothers, and I. Tinoco, Jr. 2000. Nucleic Acids: Structure, Properties and Functions. University Science Books, Sausalito, CA.

2. Li, P. T., J. Vieregg, and I. Tinoco, Jr. 2008. How RNA unfolds and refolds. *Annu. Rev. Biochem.* 77:77–100.
3. Anderson, C. F., and M. T. Record, Jr. 1995. Salt-nucleic acid interactions. *Annu. Rev. Phys. Chem.* 46:657–700.
4. Brion, P., and E. Westhof. 1997. Hierarchy and dynamics of RNA folding. *Annu. Rev. Biophys. Biomol. Struct.* 26:113–137.
5. Sosnick, T. R., and T. Pan. 2003. RNA folding: models and perspectives. *Curr. Opin. Struct. Biol.* 13:309–316.
6. Woodson, S. A. 2005. Metal ions and RNA folding: a highly charged topic with a dynamic future. *Curr. Opin. Chem. Biol.* 9:104–109.
7. Draper, D. E. 2008. RNA folding: thermodynamic and molecular descriptions of the roles of ions. *Biophys. J.* 95:5489–5495.
8. Chen, S. J. 2008. RNA folding: conformational statistics, folding kinetics, and ion electrostatics. *Annu. Rev. Biophys.* 37:197–214.
9. Rook, M. S., D. K. Treiber, and J. R. Williamson. 1999. An optimal Mg(2+) concentration for kinetic folding of the *Tetrahymena* ribozyme. *Proc. Natl. Acad. Sci. USA.* 96:12471–12476.
10. Takamoto, K., Q. He, …, M. Brenowitz. 2002. Monovalent cations mediate formation of native tertiary structure of the *Tetrahymena thermophila* ribozyme. *Nat. Struct. Biol.* 9:928–933.
11. Koculi, E., C. Hyeon, …, S. A. Woodson. 2007. Charge density of divalent metal cations determines RNA stability. *J. Am. Chem. Soc.* 129:2676–2682.
12. Soto, A. M., V. Misra, and D. E. Draper. 2007. Tertiary structure of an RNA pseudoknot is stabilized by "diffuse" Mg^{2+} ions. *Biochemistry.* 46:2973–2983.
13. Schlatterer, J. C., L. W. Kwok, …, L. Pollack. 2008. Hinge stiffness is a barrier to RNA folding. *J. Mol. Biol.* 379:859–870.
14. Lipfert, J., A. Y. Sim, …, S. Doniach. 2010. Dissecting electrostatic screening, specific ion binding, and ligand binding in an energetic model for glycine riboswitch folding. *RNA.* 16:708–719.
15. Tan, Z. J., and S. J. Chen. 2011. Importance of diffuse metal ion binding to RNA. *Met. Ions Life Sci.* 9:101–124.
16. Wu, M., and I. Tinoco, Jr. 1998. RNA folding causes secondary structure rearrangement. *Proc. Natl. Acad. Sci. USA.* 95:11555–11560.
17. Thirumalai, D. 1998. Native secondary structure formation in RNA may be a slave to tertiary folding. *Proc. Natl. Acad. Sci. USA.* 95:11506–11508.
18. Serra, M. J., and D. H. Turner. 1995. Predicting thermodynamic properties of RNA. *Methods Enzymol.* 259:242–261.
19. SantaLucia, Jr., J. 1998. A unified view of polymer, dumbbell, and oligonucleotide DNA nearest-neighbor thermodynamics. *Proc. Natl. Acad. Sci. USA.* 95:1460–1465.
20. Zhang, W. B., and S. J. Chen. 2002. RNA hairpin-folding kinetics. *Proc. Natl. Acad. Sci. USA.* 99:1931–1936.
21. Zuker, M. 2003. Mfold web server for nucleic acid folding and hybridization prediction. *Nucleic Acids Res.* 31:3406–3415.
22. Shkel, I. A., and M. T. Record, Jr. 2004. Effect of the number of nucleic acid oligomer charges on the salt dependence of stability ($\Delta G\ 37^{\circ}$) and melting temperature (Tm): NLPB analysis of experimental data. *Biochemistry.* 43:7090–7101.
23. Blake, R. D., and S. G. Delcourt. 1998. Thermal stability of DNA. *Nucleic Acids Res.* 26:3323–3332.
24. Owczarzy, R., Y. You, …, J. A. Walder. 2004. Effects of sodium ions on DNA duplex oligomers: improved predictions of melting temperatures. *Biochemistry.* 43:3537–3554.
25. Tan, Z. J., and S. J. Chen. 2008. Salt dependence of nucleic acid hairpin stability. *Biophys. J.* 95:738–752.
26. Tan, Z. J., and S. J. Chen. 2007. RNA helix stability in mixed Na^{+}/Mg^{2+} solution. *Biophys. J.* 92:3615–3632.
27. Tan, Z. J., and S. J. Chen. 2006. Nucleic acid helix stability: effects of salt concentration, cation valence and size, and chain length. *Biophys. J.* 90:1175–1190.
28. Manning, G. S. 1978. The molecular theory of polyelectrolyte solutions with applications to the electrostatic properties of polynucleotides. *Q. Rev. Biophys.* 11:179–246.
29. Gilson, M. K., K. A. Sharp, and B. Honig. 1987. Calculating the electrostatic potential of molecules in solution: method and error assessment. *J. Comput. Chem.* 9:327–335.
30. Baker, N. A., D. Sept, …, J. A. McCammon. 2001. Electrostatics of nanosystems: application to microtubules and the ribosome. *Proc. Natl. Acad. Sci. USA.* 98:10037–10041.
31. Boschitsch, A. H., and M. O. Fenley. 2007. A new outer boundary formulation and energy corrections for the nonlinear Poisson-Boltzmann equation. *J. Comput. Chem.* 28:909–921.
32. Chen, D., Z. Chen, …, G. W. Wei. 2011. MIBPB: a software package for electrostatic analysis. *J. Comput. Chem.* 32:756–770.
33. Lu, B., X. Cheng, …, J. A. McCammon. 2010. AFMPB: an adaptive fast multipole Poisson-Boltzmann solver for calculating electrostatics in biomolecular systems. *Comput. Phys. Commun.* 181:1150–1160.
34. Tan, Z. J., and S. J. Chen. 2009. Predicting electrostatic forces in RNA folding. *Methods Enzymol.* 469:465–487.
35. Grochowski, P., and J. Trylska. 2008. Continuum molecular electrostatics, salt effects, and counterion binding—a review of the Poisson-Boltzmann theory and its modifications. *Biopolymers.* 89:93–113.
36. Chen, A. A., M. Marucho, …, R. V. Pappu. 2009. Simulations of RNA interactions with monovalent ions. *Methods Enzymol.* 469:411–432.
37. Chen, A. A., D. E. Draper, and R. V. Pappu. 2009. Molecular simulation studies of monovalent counterion-mediated interactions in a model RNA kissing loop. *J. Mol. Biol.* 390:805–819.
38. Chen, A. A., and R. V. Pappu. 2007. Quantitative characterization of ion pairing and cluster formation in strong 1:1 electrolytes. *J. Phys. Chem. B.* 111:6469–6478.
39. Tan, Z. J., and S. J. Chen. 2005. Electrostatic correlations and fluctuations for ion binding to a finite length polyelectrolyte. *J. Chem. Phys.* 122:44903.
40. Tan, Z. J., and S. J. Chen. 2006. Ion-mediated nucleic acid helix-helix interactions. *Biophys. J.* 91:518–536.
41. Tan, Z. J., and S. J. Chen. 2006. Electrostatic free energy landscapes for nucleic acid helix assembly. *Nucleic Acids Res.* 34:6629–6639.
42. Tan, Z. J., and S. J. Chen. 2008. Electrostatic free energy landscapes for DNA helix bending. *Biophys. J.* 94:3137–3149.
43. Chen, G., Z. J. Tan, and S. J. Chen. 2010. Salt-dependent folding energy landscape of RNA three-way junction. *Biophys. J.* 98:111–120.
44. Tan, Z. J., and S. J. Chen. 2010. Predicting ion binding properties for RNA tertiary structures. *Biophys. J.* 99:1565–1576.
45. Misra, V. K., and D. E. Draper. 2002. The linkage between magnesium binding and RNA folding. *J. Mol. Biol.* 317:507–521.
46. Misra, V. K., R. Shiman, and D. E. Draper. 2003. A thermodynamic framework for the magnesium-dependent folding of RNA. *Biopolymers.* 69:118–136.
47. Li, P. T., and I. Tinoco, Jr. 2009. Mechanical unfolding of two DIS RNA kissing complexes from HIV-1. *J. Mol. Biol.* 386:1343–1356.
48. Su, L., L. Chen, …, A. Rich. 1999. Minor groove RNA triplex in the crystal structure of a ribosomal frameshifting viral pseudoknot. *Nat. Struct. Biol.* 6:285–292.
49. Conn, G. L., A. G. Gittis, …, D. E. Draper. 2002. A compact RNA tertiary structure contains a buried backbone-K^{+} complex. *J. Mol. Biol.* 318:963–973.
50. Westhof, E., and M. Sundaralingam. 1986. Restrained refinement of the monoclinic form of yeast phenylalanine transfer RNA. Temperature factors and dynamics, coordinated waters, and base-pair propeller twist angles. *Biochemistry.* 25:4868–4878.
51. Holland, J. A., M. R. Hansen, …, D. W. Hoffman. 1999. An examination of coaxial stacking of helical stems in a pseudoknot motif: the gene 32 messenger RNA pseudoknot of bacteriophage T2. *RNA.* 5:257–271.

52. Shen, L. X., and I. Tinoco, Jr. 1995. The structure of an RNA pseudoknot that causes efficient frameshifting in mouse mammary tumor virus. *J. Mol. Biol.* 247:963–978.

53. Weixlbaumer, A., A. Werner, …, R. Schroeder. 2004. Determination of thermodynamic parameters for HIV DIS type loop-loop kissing complexes. *Nucleic Acids Res.* 32:5126–5133.

54. Ennifar, E., P. Walter, …, P. Dumas. 2001. Crystal structures of coaxially stacked kissing complexes of the HIV-1 RNA dimerization initiation site. *Nat. Struct. Biol.* 8:1064–1068.

55. Lu, X. J., and W. K. Olson. 2003. 3DNA: a software package for the analysis, rebuilding and visualization of three-dimensional nucleic acid structures. *Nucleic Acids Res.* 31:5108–5121.

56. Bukhman, Y. V., and D. E. Draper. 1997. Affinities and selectivities of divalent cation binding sites within an RNA tertiary structure. *J. Mol. Biol.* 273:1020–1031.

57. Römer, R., and R. Hach. 1975. tRNA conformation and magnesium binding. A study of a yeast phenylalanine-specific tRNA by a fluorescent indicator and differential melting curves. *Eur. J. Biochem.* 55: 271–284.

58. Nixon, P. L., and D. P. Giedroc. 1998. Equilibrium unfolding (folding) pathway of a model H-type pseudoknotted RNA: the role of magnesium ions in stability. *Biochemistry.* 37:16116–16129.

59. Theimer, C. A., and D. P. Giedroc. 2000. Contribution of the intercalated adenosine at the helical junction to the stability of the gag-pro frameshifting pseudoknot from mouse mammary tumor virus. *RNA.* 6:409–421.

60. Qiu, H., K. Kaluarachchi, …, D. P. Giedroc. 1996. Thermodynamics of folding of the RNA pseudoknot of the T4 gene 32 autoregulatory messenger RNA. *Biochemistry.* 35:4176–4186.

61. Bai, Y., M. Greenfeld, …, D. Herschlag. 2007. Quantitative and comprehensive decomposition of the ion atmosphere around nucleic acids. *J. Am. Chem. Soc.* 129:14981–14988.

62. Bai, Y., V. B. Chu, …, S. Doniach. 2008. Critical assessment of nucleic acid electrostatics via experimental and computational investigation of an unfolded state ensemble. *J. Am. Chem. Soc.* 130:12334–12341.

63. Stellwagen, E., J. M. Muse, and N. C. Stellwagen. 2011. Monovalent cation size and DNA conformational stability. *Biochemistry.* 50:3084–3094.

64. Patra, C. N., and A. Yethiraj. 2000. Density functional theory for the nonspecific binding of salt to polyelectrolytes: thermodynamic properties. *Biophys. J.* 78:699–706.

65. Grilley, D., A. M. Soto, and D. E. Draper. 2009. Direct quantitation of Mg^{2+}-RNA interactions by use of a fluorescent dye. *Methods Enzymol.* 455:71–94.

66. Grilley, D., V. Misra, …, D. E. Draper. 2007. Importance of partially unfolded conformations for Mg(2+)-induced folding of RNA tertiary structure: structural models and free energies of Mg^{2+} interactions. *Biochemistry.* 46:10266–10278.

67. Leipply, D., D. Lambert, and D. E. Draper. 2009. Ion-RNA interactions thermodynamic analysis of the effects of mono- and divalent ions on RNA conformational equilibria. *Methods Enzymol.* 469:433–463.

68. Leipply, D., and D. E. Draper. 2011. Effects of Mg^{2+} on the free energy landscape for folding a purine riboswitch RNA. *Biochemistry.* 50:2790–2799. 10.1021/bi101948k.

69. Lambert, D., D. Leipply, …, D. E. Draper. 2009. The influence of monovalent cation size on the stability of RNA tertiary structures. *J. Mol. Biol.* 390:791–804.

70. Moghaddam, S., G. Caliskan, …, S. A. Woodson. 2009. Metal ion dependence of cooperative collapse transitions in RNA. *J. Mol. Biol.* 393:753–764.

71. Vieregg, J., W. Cheng, …, I. Tinoco, Jr. 2007. Measurement of the effect of monovalent cations on RNA hairpin stability. *J. Am. Chem. Soc.* 129:14966–14973.

72. Stellwagen, E., Q. Dong, and N. C. Stellwagen. 2007. Quantitative analysis of monovalent counterion binding to random-sequence, double-stranded DNA using the replacement ion method. *Biochemistry.* 46:2050–2058.